The role of far-red fluorescing chlorophylls in the quenching of LHCII

Václav Šebelík[1], Alexander Paradzah[1], David Bína[1,2], Dan-Hong Li[3], Valentyna Kuznetsova[1], Alexander Ruban[3,*], Tomáš Polívka[1,*]

[1]Department of Physics, Faculty of Science, University of South Bohemia, Branišovská 1760, 370 05 České Budějovice, Czech Republic

[2] Biology Centre of the Czech Academy of Sciences, Branišovská 31, 370 05 České Budějovice, Czech Republic

[3] School of Biological and Behavioural Sciences, Queen Mary University of London, Mile End Road, London E1 4NS, United Kingdom

* Corresponding authors: tpolivka@prf.jcu.cz, a.ruban@qmul.ac.uk

ORCID IDs:

Václav Šebelík	0000-0002-9597-3117
Alexander Paradzah	0000-0002-4200-8567
David Bína	0000-0002-9259-4218
Dan-Hong Li	0000-0003-4469-1192
Valentyna Kuznetsova	0000-0001-9858-4283
Alexander Ruban	0000-0001-8554-0249
Tomáš Polívka	0000-0002-6176-0420

Keywords

LHCII, non-photochemical quenching, far-red chlorophyll fluorescence, energy dissipation, transient absorption spectroscopy

Acknowledgment

The authors from University of South Bohemia thank the Czech Science foundation grant 24-11344S and OP JAK project Photomachines reg. no. CZ.02.01.01/00/22_008/0004624.

Abstract

In photosynthetic organisms, the major light-harvesting antenna protein LHCII performs the dual function of capturing excitation energy and protecting the photosystem from over-excitation via non-photochemical quenching (NPQ). We investigated the role of far-red-fluorescing chlorophylls (emission >700 nm) in quenching LHCII by comparing isolated trimeric LHCII (denoted F680) with aggregated LHCII prepared in a glycerol-rich medium (denoted F730). Time-resolved fluorescence and ultrafast transient-absorption spectroscopy, including an intensity-cycling scheme to separate annihilation-free dynamics, were used. We find that the red-emissive chlorophyll states are populated in <100 ps and display properties consistent with states having a low transition-dipole moment. Despite the significant shortening of the chlorophyll-*a* excited-state lifetimes in the F730 sample (hundreds of picoseconds vs. several nanoseconds in F680), no long-lived excited-state species attributable to the far-red emitters were detected in the transient-absorption data. These findings suggest that the far-red-fluorescing chlorophylls are not the direct quenchers but rather markers of the quenched LHCII configuration and highlight the necessity to better define aggregate size and internal organization for elucidating the molecular mechanism of quenching.

Introduction

Photosynthesis is a process by which plants, algae, and some bacteria convert light energy into chemical energy, powering life on Earth. All photosynthetic organisms use specialized light-harvesting antenna proteins to absorb light and transfer its energy to the photosynthetic reaction centers. Unlike the reaction centers, there is a large diversity of light-harvesting complexes among photosynthetic organisms (Croce and Van Amerongen 2014; Mirkovic et al. 2017). In addition to light harvesting, some antenna proteins play a crucial role in protecting the photosynthetic apparatus from photodamage under excess light conditions (Ruban 2016). In plants and algae, the light-harvesting complex II (LHCII) associated with Photosystem II is the key protein that can switch between light-harvesting and photoprotective states. This ensures the proper regulation of energy flow from the antenna to the reaction center of Photosystem II (Ruban 2016). LHCII binds chlorophyll *b* (Chl-*b*), chlorophyll *a* (Chl-*a*), and four carotenoids: two luteins, violaxanthin, and neoxanthin (Liu et al. 2004).

The switch between light-harvesting (unquenched) and photoprotective (quenched) states of LHCII is a complex process driven by changes in proton gradient across thylakoid membrane, involves other proteins such as PsbS (Ruban 2016) and is also associated with conversion between two xanthophyll cycle carotenoids, violaxanthin and zeaxanthin (Demmig-Adams 1990; Peterman et al. 1997). In the quenched state, excess energy is dissipated as a heat in a process called non-photochemical quenching, which is manifested by significant shortening of Chl-*a* excited state lifetime. While in light-harvesting state isolated LHCII has a lifetime of about 4 ns, the Chl-*a* lifetime drops below 1 ns when LHCII switches to the photoprotective conformation (Mullineaux et al. 1993; Belgio et al. 2012). Single molecular spectroscopy identified the conformational switch by clear spectral changes associated with transition from unquenched and quenched states (Krüger et al. 2010; Schlau-Cohen et al. 2015), but the exact nature of the structural changes associated with the switch remains unknown. It is known, however, that X-ray diffraction structure of LHCII represents likely the quenched state (Pascal et al. 2005) and at level of individual LHCII complexes, twist of the carotenoid terminal ring has been suggested as a possible cause of the switch between quenched and unquenched state (Liguori et al. 2017). Recent comparison of the cryo-EM structures of LHCII in quenched and unquenched states revealed some differences in the orientation of A and B helixes and the positions and structure of amphipathic helixes D cand E with alteration in some hydrogen bonding patterns at the luminal site of the complex (Ruan et al. 2023; Ruban 2024).

These changes in the structure of LHCII have been suggested to be the causes of some observed spectral changes mentioned above.

The quenching mechanism operating in LHCII is also a matter of considerable debate. Energy transfer from the Q_y state of Chl-*a* to the lowest excited state of carotenoid in LHCII was proposed more than 30 years ago (Frank et al. 1994), and experimental evidence of such mechanism was reported later in LHCII (Ruban et al. 2007) and in cyanobacterial ancestor of LHCII (Staleva et al. 2015). Yet, other quenching mechanisms in LHCII, involving electron transfer between Chl-*a* and carotenoid (Holt et al. 2005), Chl-Car excitonic coupling (Bode et al. 2009) or Chl-Chl charge transfer states (Müller et al. 2010), have been proposed.

The increased energy dissipation in LHCII is often marked by presence of red shifted fluorescence bands at 77 K appearing in the 700-740 nm spectral region (Ruban et al. 1991; Miloslavina et al. 2008). These bands, denoted here as F700 and F730 (Wilson et al. 2022), though more red fluorescence bands were identified in various LHCII aggregates (Ostroumov et al. 2020), are weak in isolated LHCII, but are stabilized and enhanced upon LHCII aggregation occurring at low detergent levels (Mullineaux et al. 1993). Temperature-dependent fluorescence data demonstrated that at room temperature the red fluorescence bands are weak, their intensity gradually increases down to 80 K but may decrease again at even lower temperatures (Chmeliov et al. 2019). Interestingly, time-resolved fluorescence data showed that while the 680 nm fluorescence is heavily quenched in LHCII aggregates, chlorophylls responsible for F700 and F730 fluorescence have a lifetime of 2-3 ns, corresponding to unquenched Chl-*a* (Chmeliov et al. 2019; Wilson et al. 2022; Yao et al. 2022). This suggests that the red emitting Chls are not the quenchers, but their presence is rather an indicator of the quenched state of LHCII (Chmeliov et al. 2016; Mascoli et al. 2020). The origin of the 77 K red emission in LHCII has not been settled yet, though Chl charge transfer (CT) states are the most favorable explanation (Müller et al. 2010; Wahadoszamen et al. 2012; Chmeliov et al. 2019; Ostroumov et al. 2020; Mascoli et al. 2020). Alternatively, Chl excimers (Wilson et al. 2022, Zou et al. 2025) have been suggested as a possible origin.

While fluorescence-based methods have been widely used to study properties of LHCII aggregates (Kirchhoff et al. 2003; Miloslavina et al. 2008; Chmeliov et al. 2016, 2019; Tutkus et al. 2021), transient absorption spectroscopy, which can achieve significantly better time resolution, has been only scarcely used. Main reason is high photon excitation density used typically in transient absorption experiments, resulting in significant annihilation phenomena in aggregated LHCII (Barzda et al. 2001; Müller et al. 2010; Van Oort et al. 2018). Including

annihilation to the data fitting and modelling may help (Ruban et al. 2007), but it makes determination of annihilation-free dynamics challenging. Recently, an intensity-cycling method using a simple experimental protocol to extract annihilation-free dynamics from data has been developed (Malý et al. 2023) and successfully used for a few systems including LHCII (Malý et al. 2023; Lee et al. 2024).

Here we apply time-resolved fluorescence and transient absorption spectroscopy to compare isolated LHCII trimers and LHCII aggregates prepared from LHCII incubated in a glycerol-rich medium (Wilson et al. 2022) exhibiting unusually strong emission at wavelengths longer than 700 nm at 77 K. In transient absorption experiment, we use the intensity cycling method to test the involvement of annihilation in the observed dynamics. Our data show that the red emissive states of Chl-*a* are populated in less than 100 ps and are likely associated with states having a weak transition dipole moment.

Materials and Methods

LHCII was isolated from dark-adapted (45 min) spinach leaves obtained commercially. PSII-enriched BBY thylakoid membranes (Ruban et al. 1994; Shukla et al. 2020) were solubilized with 0.6 % (*w*/*v*) n-dodecyl-β-D-maltoside (β-DDM) (Sigma-Aldrich) at 1 mg·mL^{-1} Chl for 45 minutes, then separated on a sucrose density gradient (0.16–1.87 M) by ultracentrifugation (Beckman Coulter Optima L-80 XP, SW41Ti) 40,000 rpm for 17.5 hours at 4 °C. Isolated LHCIIs were desalted using a PD-10 column (Cytiva, UK) with buffer containing 60 mM HEPES (pH 7.6), 30 mM NaCl, and 0.03% β-DDM and flash-frozen in liquid nitrogen. All experiments (at room temperature and 77 K) were performed on samples containing 67 % *v*/*v* glycerol. To ensure the aggregation-free state and to offset the effect of dilution of detergent by glycerol, the final concentration of β-DDM was adjusted to 0.6 % for the trimeric (not aggregated) LHCII sample (labelled F680 in the following) after mixing with glycerol. Prior to measurements, the sample was incubated for 24 hours in the dark at 21°C. The aggregated sample with maximum development of the red-shifted spectral features (F730) was prepared by first diluting 0.6 mL stock LHCII with glycerol to final volume of 1.8 mL. Following a 22-hour incubation in the dark (at 21°C), the detergent was removed by 2–3 hours treatment by 800 mg Biobeads SM-2 (BioRad). Following low-speed centrifugation to separate Biobeads, the sample was removed using a Pasteur pipette and stored on ice. Optical density of the

samples used for transient absorption experiments were 0.6 (F680) and 0.25 (F730) at the Chl-*a* Q_y maximum in a 2-mm cuvette.

The quality of the preparations (development of the red states and presence of fluorescence quenching in F730 and the absence of both in F680) was verified by emission spectroscopy at 77 K and time-resolved fluorescence at room-temperature and 77 K. All fluorescence measurements were performed using the FluoTime 300 instrument (PicoQuant, Germany). Experiments at cryogenic temperature were done on samples immersed in liquid nitrogen using custom-built Dewar vessel or the OptistatDN2 cryostat. Fluorescence was detected using front-face illumination from a thin-layer sample placed in a locally built holder (Dewar) or a purpose-built plastic cuvette (cryostat). The room-temperature recordings were performed in 1 cm × 1 cm quartz cuvettes in right-angle geometry. Excitation wavelength for all fluorescence experiments was 480 nm. The FWHM of the instrument response function as recorded with Ludox scatterer is <190 ps, and deconvolution of IRF allows to reliable determine time constants >50 ps (Alster et al. 2024).

Triplet-minus-singlet spectra were acquired using the locally built kinetics spectrophotometer described in detail previously (Bína et al. 2006). Triplet states were generated by 2 μs broadband pulses delivered by a xenon flashlamp.

For ultrafast transient absorption experiments, a Spitfire Ace regenerative amplifier system (Spectra Physics), powered by a Ti:sapphire oscillator (MaiTai SP, Spectra Physics) and a Nd:YLF laser (Empower 30, Spectra Physics), was used to generate both excitation (pump) and probe pulses. This system produced 4 mJ pulses at a central wavelength of 800 nm, with a repetition rate of 1 kHz and a pulse duration of approximately 100 fs. The excitation beam was generated via parametric amplification using a TOPAS Prime (Light Conversion). The pump beam was focused onto the sample using a 300 mm focal length lens, and its intensity was adjusted to a range of 70–100 μW. A portion of the 800 nm beam from the Spitfire Ace was directed to a home-built non-collinear optical parametric amplifier, which generated a 1200 nm beam. This beam was then focused onto a 2 mm CaF_2 plate to produce a white-light supercontinuum (WLC) probe beam. A Berek polarizer was used to set the relative polarization between the pump and probe beams to the magic angle. To improve the signal-to-noise ratio, the WLC was split into reference and probe beams, both of which were detected using a dual CCD array in a prism spectrograph. This setup enabled data collection across a broad spectral range from 450 to 900 nm. A liquid nitrogen bath cryostat (Optistat DN2, Oxford Instruments, UK) was used for transient-absorption experiments performed at 77 K. All transient absorption

data were collected in 2-mm quartz (room temperature) or 1-mm plastic (77 K) cuvettes. To avoid photodamage, microstirrer was used for all room temperature measurements.

Room temperature intensity-cycling measurements were performed at three pulse energies for each sample. The F680 sample was pumped at 41, 123, and 164 μJ/cm^2 while the F730 sample was pumped at 123, 367, and 489 μJ/cm^2 pulse fluences. Pure third-order nonlinear ($PP^{(3)}$) and fifth-order nonlinear ($PP^{(5)}$) signals were obtained by arithmetically combining the three datasets (see the Results section). Furthermore, a pump pulse fluence of 41 μJ/cm² was utilized for the F730 sample, and kinetics were compared to the kinetics of $PP^{(3)}$ to evaluate the effectiveness of extracting the pure third-order nonlinear dynamics. $PP^{(3)}$ kinetics should not decay faster than kinetics obtained from low pump fluences if the extraction of third-order nonlinear dynamics is successful. For the F680 sample, the 41 μJ/cm², which is the lowest of the three pump fluences, was used for this test.

The resulting data sets from transient absorption measurements were analyzed using CarpetView software (Light Conversion, Lithuania) and fitted with a sequential model to obtain evolution-associated difference spectra (EADS) (Van Stokkum et al. 2004). To determine the annihilation constants for each dataset from the intensity-cycling measurements, we fitted the $PP^{(3)}$ and $PP^{(5)}$ kinetics using a fitting routine in Python. First, the decay kinetic of the $PP^{(3)}$ datasets averaged over the maximum of the Chl-*a* Q_y band, from 665 to 683 nm, were fit with an exponential decay function. The fitting parameters obtained from the $PP^{(3)}$ fit were used to construct the decay kernel used in fitting the $PP^{(5)}$ decay kinetic, also obtained from averaging over the Chl-*a* band, to determine the annihilation constants. Further information is provided in the Results section.

Results

Steady-state Spectroscopy

Absorption spectra of the F680 and F730 samples were recorded at 77 K and room temperature (Fig. 1). There are no significant differences between absorption spectra of both samples; they show well-defined Chl-*a* spectral signatures in the Soret region centered at approximately 435 nm and in the Q_y band peaking at 675 nm. The presence of Chl-*b* in LHCII is manifested as absorption peaks around 650 nm (Q_y) and 473 nm (Soret), which is superimposed onto the carotenoid absorption bands that covers the 400-500 nm spectral range. Clearly, the two samples have the same pigment composition, so no pigment loss occurs during

the aggregation process. At 77 K, the overall shape of absorption spectra of both samples is qualitatively similar to room temperature, except the spectral bands are sharper at cryogenic temperature. This is particularly pronounced in the Q_y band where shoulders at 670 and 660 nm indicate Chl spectral heterogeneity at 77 K. Notably, no red-shifted absorption bands in the F730 sample are observed.

Fluorescence spectra, shown also in Fig. 1, exhibit markedly different behavior compared to absorption. While at room temperature the F680 and F730 samples are similar, having maximum at 684 nm accompanied by a vibrational shoulder at 740 nm, decreasing temperature

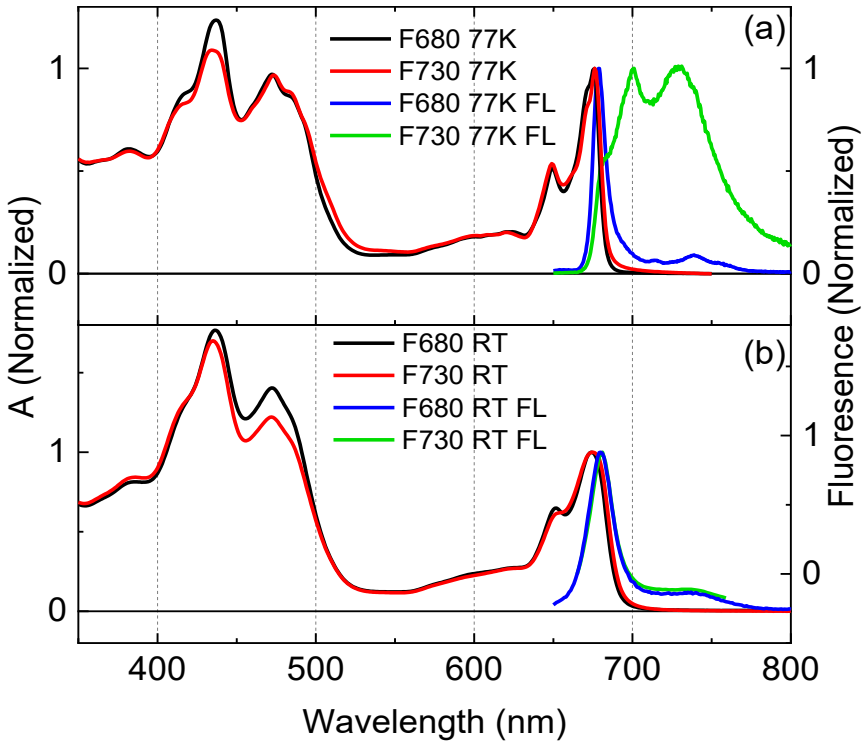

Figure 1. Normalized absorption spectra (black and red lines) for the F680 and F730 samples at 77 K (a) and RT (b). The spectra are normalized at the maximum of the Q_y band of Chl-*a*. The blue and green lines show normalized fluorescence spectra. The fluorescence spectra were measured after excitation at 480 nm.

to 77 K reveals the distinct emission properties of F680 and F730. The F680 sample has typical shape of low temperature LHCII fluorescence with single sharp peak at 681 nm. For F730 however, the 'normal' 680 nm emission is suppressed and new peaks at 700 and 730 nm appear, indicating aggregation of LHCII in agreement with previous studies (Kirchhoff et al. 2003; Wilson et al. 2022).

Table 1. Fluorescence parameters of the F680 and F730 sample obtained at ambient and cryogenic temperature. SD of lifetimes was ~10 %, computed from four replicates (hence it combines both the error of the fit and the sample-to sample variability). For the F680 sample, decay of which was monoexponential, the detection was at 680 nm. For the F730 sample, the data were extracted from the global analysis of the spectrally resolved fluorescence decay data. For an example of corresponding decay-associated spectra of the F730 samples see Fig. 3.

F680	RT	4 ns			
	77 K	6.3 ns			
F730	RT	< 50 ps	120 ps	550 ps	1 ns
	77 K	< 50 ps	170 ps	1.8 ns	3.9 ns

Time-resolved fluorescence

The Chl-*a* fluorescence decay data are shown in Fig. 2. Time constants associated with the decays are summarized in Table 1. The fluorescence decay of the F680 LHCII sample is satisfactorily described by a single exponential with a lifetime of 4 ns at room temperature that prolongs to 6.3 ns at 77 K. In contrast, F730 LHCII exhibits much shorter lifetime of Chl-*a* emitting at 680 nm, exhibiting multi-exponential decay with dominant decay components shorter than 200 ps at both room temperature and 77 K, respectively (Table 1). The example spectra pertaining to the lifetime components (i.e. the decay-associated spectra, DAS) and the corresponding average lifetimes for the F730 LHCII at room and cryogenic temperature are shown in Fig. 3. At room temperature, the F730 LHCII exhibits negligible spectral development in time, with all the DAS having almost identical shape. In contrast, at 77 K, the DAS clearly evolved with lifetime, with the longer-lifetime components exhibiting progressive red shift. This information is condensed in the average lifetime plots in Fig 3. The average lifetime of the room-temperature sample shows the value of ~670 nm, independent of temperature while at 77 K, there is a clear shift from ~1 ns to well over 3 ns lifetime occurring at 685-700 nm region.

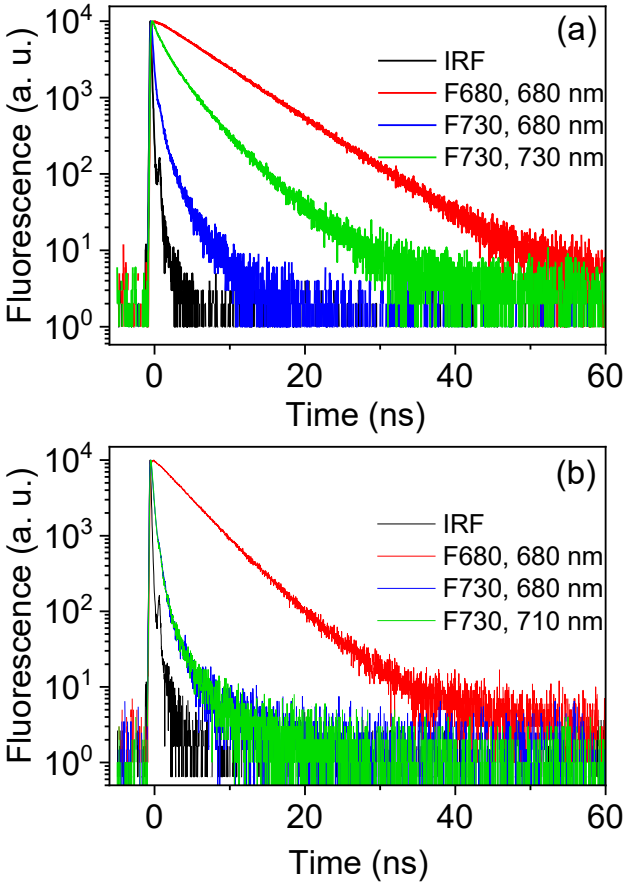

Figure 2. Fluorescence decays of F680 and F730 samples at 77 K (a) and 293 K (b).

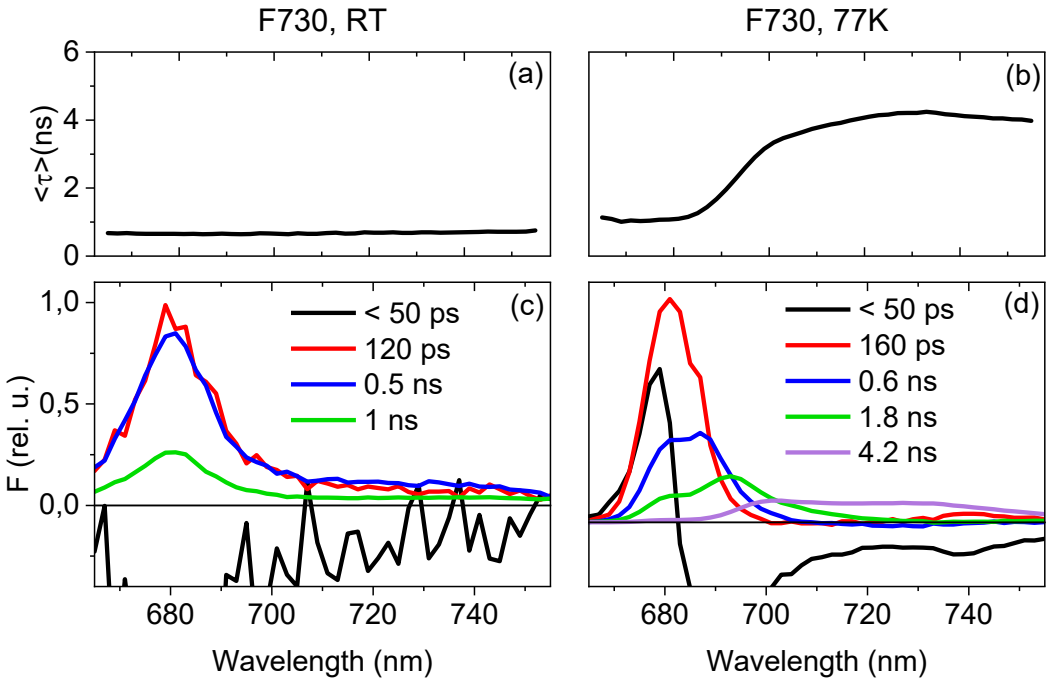

Figure 3. The average lifetime (a,b, intensity-weighted) and decay-associated spectra (along with lifetimes, c,d) acquired on the F730 LHCII sample at ambient (a,c) and cryogenic (b,d) temperature.

Focusing on the shape of DAS in more detail, the eponymous 730 nm peak is found only at 77 K in the slowest, ~4 ns component, accompanied by a peak or shoulder at 700 nm. The ratio of amplitudes of these two features was about 1, varying slightly between different preparations. Of the shorter lifetime DAS, the fastest one, <50 ps (black DAS), which is at the limit of the time resolution of the apparatus, contains dynamic processes involving intra-complex energy transfer between pigments and equilibration within Chl-*a* pool in LHCII as evidenced by the derivative shape corresponding to a decay at the blue part and rise at red part of the 680 nm fluorescence band. Indeed, this is the only component showing a significant negative part clearly indicative of energy transfer. The other three DAS, 160 ps (red), 600 ps (blue), 1.8 ns (green) and ~4 ns (magenta), have positive amplitude in the whole spectral range thus all exhibit only decay. However, the second fastest, ~160 ps, component clearly approaches zero in the 700-730 nm region which can be attributed to mutual cancelling of positive (fluorescence decay) and negative (fluorescence increase) amplitudes. In case of the energy transfer, the asymmetry between the area of the positive and negative part of a DAS can be interpreted as the acceptor state having a smaller transition dipole moment, or that the decay component corresponds to a branched path in which part of the energy goes to a nonfluorescent state.

Overall, the observed behavior of time-resolved fluorescence, including the absence of clear indication of energy transfer is comparable to that reported earlier for LHCII complexes exhibiting 730 nm fluorescence at 77 K (Miloslavina et al. 2008; Natali et al. 2016; Mascoli et al. 2020).

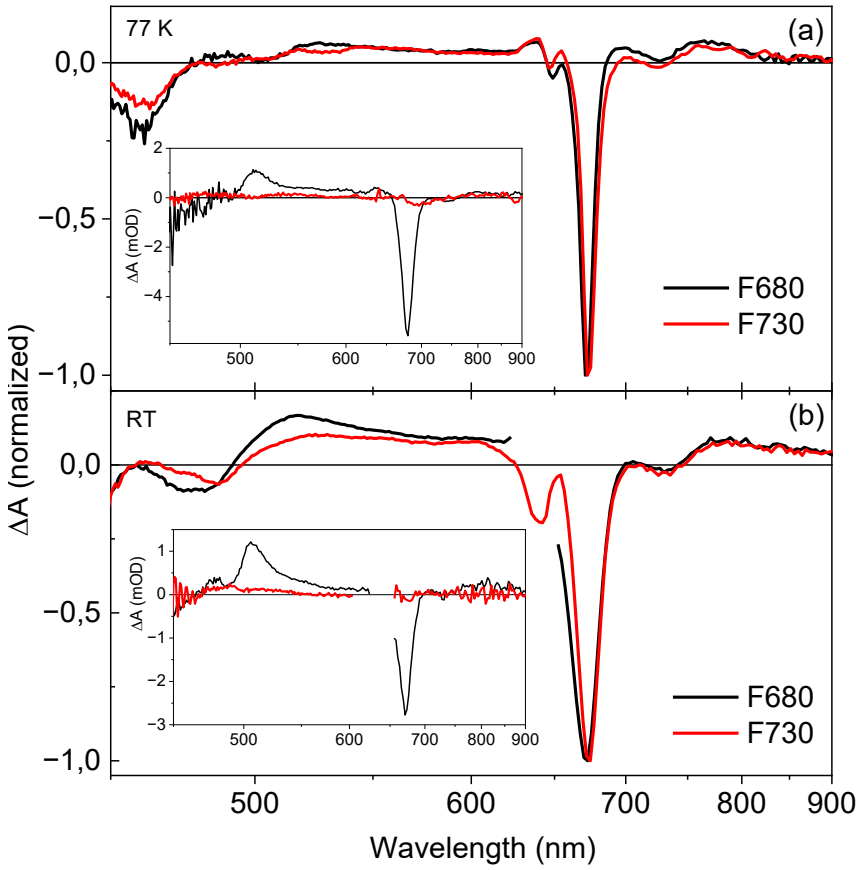

Figure 4. Transient absorption spectra at 1 ps after Chl-*b* excitation at 645 nm. Spectra are measured at 77 K (a), and room temperature (b). All spectra are normalized at the maximum Chl-*a* Q_y bleach. Insets show transient absorption spectra at 2 ns demonstrating a carotenoid triplet signal appearing at long delays exclusively for F680 LHCII. RT F630 to 650 nm data removed due to pump scattering.

Transient absorption spectroscopy

We performed pump-probe transient absorption spectroscopy at room temperature and at 77 K to explore the ultrafast excited state dynamics of the F680 and F730 LHCII. The excitation wavelengths were chosen to excite the Chl-*b* Q_y band at 645 and 650 nm and dynamics were monitored in the 450 – 900 nm window. Excitation of Chl-*b* to the Q_y band enables a clearer view of the Chl-*a* dynamics because Chl-*b* transfers the excitation to Chl-*a* which dynamics can then be studied without contamination from the pump scattering. Fig. 4 shows the transient absorption spectra recorded at 1 ps delay for both samples at 77 K and room temperature. Raw data showing the time evolution of spectra are shown in Supporting Information (Fig. S1). The spectra show characteristic LHCII features with Chl bleaching signals accompanied by broad ESA features in the 500-630 nm spectral range (Polívka et al. 2002; Saccon et al. 2020). At

longer wavelengths, the spectra show a Chl-*a* stimulated emission vibrational band at ~ 730 nm and a broad ESA feature extending to about 900 nm. At 1 ps delay, the well-developed Chl-*a* bleaching is due to excitation energy transfer from Chl-*b*, and direct Chl-*a* excitation. Comparing the spectra recorded at 1 ps and 0.2 ps (Fig. S1), for instance, shows a reduction in the Chl-*b* bleaching in the Soret band with a corresponding increase in the Chl-*a* bleach, corroborating the assertion of fast Chl-*b* to Chl-*a* energy transfer.

Insets in both panels of Fig. 4 show the 77 K and RT spectra recorded at 2 ns. In both cases, it is observed that the F730 Chl-*a* Q_y bleach, as well as other spectral features, have completely decayed over this timescale. The F680 sample, however, still exhibits a well-defined Chl-*a* bleaching in the Q_y band and a prominent carotenoid triplet signal peaking at 505 nm. The triplet signal in the F680 sample emerges at ns-timescales with a rise time that correlates with the decay rate of the Chl-*a* Q_y band signal. This shows that carotenoid triplets quench the Chl-*a* pigments in the F680 LHC II trimers. The fast decay of the F730 LHCII and the absence of a carotenoid triplet signal suggest that a different quenching mechanism is responsible for energy dissipation in F730.

At 1 ps after excitation, there is no significant difference in transient absorption spectra of F680 and F730 LHCII at 77 K, contrasting to the dramatic changes observed in fluorescence spectra (Fig. 1). We do not detect any additional stimulated emission signal in the 700-750 nm spectral region that could be expected due to the increased 77 K fluorescence of the F730 LHCII. There is a 3 nm red shift of the Q_y bleaching for the F730 at 77 K, but similar shift is observed also at room temperature. It is important to note that energy equilibration within the Chl pools takes longer than 5 ps (Fig. S2), thus at 1 ps we look at non-equilibrated Chl-*a* pool. Yet, the small red shift in bleaching maximum is maintained even at longer delays (Fig. S3). The data thus indicate that at early times after excitation, F680 and F730 exhibit similar behavior. Transient absorption spectra at longer delay, 100 ps, are shown in Fig. 5. At 77 K, the Chl-*a* bleaching band of F730 has a distinct red shoulder extending beyond 700 nm, which is clearly absent in F680. Moreover, this shoulder is not present at room temperature as evidenced by the spectra shown in the inset of Fig. 5. The shoulder is thus formed only at longer delays and is likely due to stimulated emission associated with red fluorescence observed exclusively at 77 K (Fig. 1).

Despite only mild differences between F680 and F730 transient absorption spectra, kinetics measured at Chl-*a* bleaching maximum (Fig. 6) reveal completely different dynamics, mirroring the observations obtained from time resolved fluorescence. At both temperatures, the

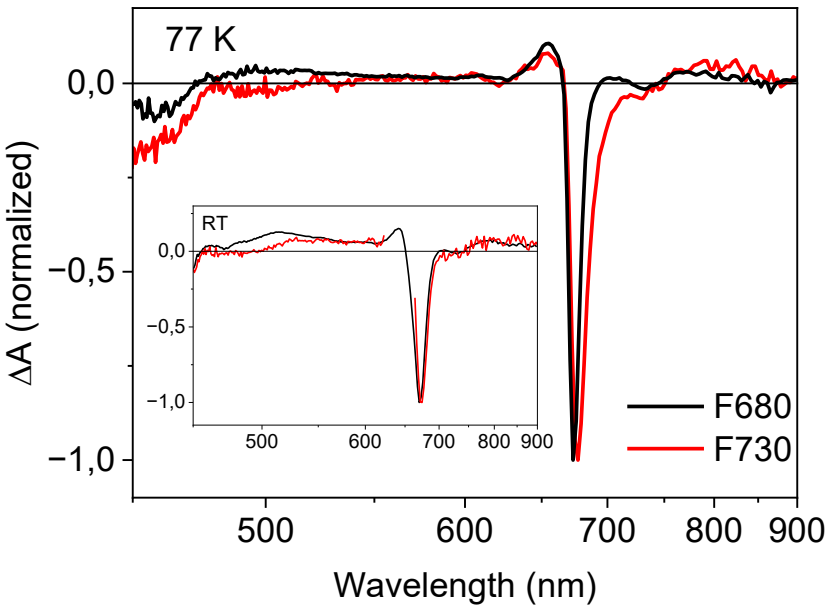

Figure 5. Normalized transient absorption spectra measured at 77 K 100 ps after excitation of Chl-*b* at 645 nm for F680 (black) and F730 (red). Inset shows the same data measured at room temperature.

F730 Chl-*a* Q_y decay is significantly faster, decaying to nearly zero signal within 0.5 ns. F680, in contrast decays with 'standard' LHCII kinetics having a time constant about 2 ns. Changes induced by going from room temperature to 77 K are negligible in both F680 and F730 as the Chl-*a* lifetime is only slightly longer at 77 K.

The lifetimes associated with Chl dynamics were estimated from global fitting analysis. A 5-compartment sequential model was required to fit the F680 datasets at both 77 K and RT, while the F730 datasets were fit using a 4-compartment sequential model as F730 does not contain any long-lived signal that does not decay within the time window of the experiment. From the sequential analysis, we obtain the evolution-associated difference spectra (EADS) and their associated lifetimes (Fig. S4). The spectra exhibit well-defined Chl-*a* Q_y bleach signals, arising from direct excitation of the Q_x/vibrational band of Chl-*a* at 645 nm, and broad ESA features below 650 nm and ~750-900 nm regions. No major differences are observed in the zero-time spectra across the samples, both at 77 K and RT. The zero-time spectra decay with lifetimes of approximately 0.5 ps across all the samples. The second EADS, which emerges in ~ 0.5 ps, are characterized by substantially reduced Chl-*b* bleach and associated increases in the Chl-*a* Q_y signal. In the F680 samples, the second EADS have lifetimes of 5.7 and 3.7 ps at 77 K and RT, respectively.

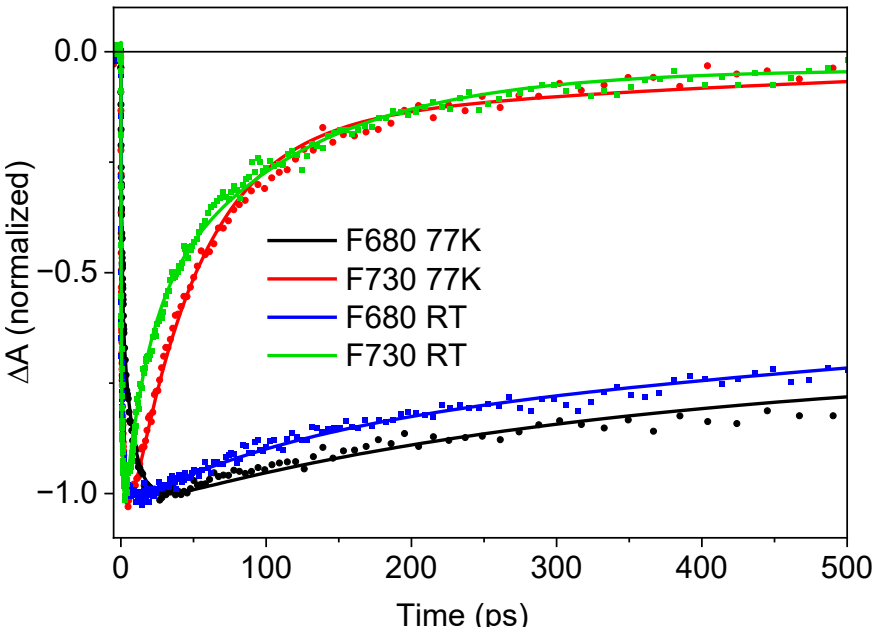

Figure 6. Normalized Chl-*a* kinetic traces after excitation of the Chl-*b* Q_y band. The kinetics are normalized, and solid lines represent multi-exponential decay fits from global analysis.

Corresponding lifetimes for the F730 samples are comparable, yielding 3.5 and 1.4 ps. The lifetimes associated with the second EADS likely represent equilibration within Chl-*a* pool. As a result, the third EADS have red-shifted Chl-*a* bleaching band. Again, this is observed in both samples. It is important to note, however, that energy equilibration within the Chl-*a* pigments is not complete within 5 ps, as shown in Fig. S2, depicting the time-dependence of the position of Qy bleaching maximum. In F680, the third EADS have lifetimes of 56 and 86 ps at 77 K and RT, respectively. Corresponding lifetimes in F730 are 54 and 22 ps. The amplitude of this component is much larger for F730 as evidenced by significantly larger reduction of the Chl-*a* bleaching signal in F730 compared to F680 and these lifetimes likely contain some annihilation component (see below). The dynamics of the F730 samples are complete with the fourth EADS decaying in 670 and 176 ps at 77 K and RT, respectively. It is worth noting that the 670 ps EADS of F730 at 77 K contains the red shoulder at the Chl-*a* bleaching band, while no such shoulder is evident in the preceding 56 ps EADS. This implies that the red shoulder, presumably associated with the red emission bands at 77 K, is formed at a time scale of tens of picoseconds. In F680 samples, the fourth EADS have lifetimes of 2 and 2.4 ns at 77 K and RT, and decay into the fifth, non-decaying EADS.

Exciton annihilation in F680 and F730 samples at room temperature

The data presented in the previous paragraphs clearly show that F730 LHCII is heavily quenched as its Chl-*a* lifetime shortens far below 0.5 ns. However, since F730 LHCII is

supposed to be aggregated, to achieve single-exciton dynamics and at the same time obtain a reasonable signal-to-noise ratio in pump-probe measurements is challenging. Excitation intensities used in these experiments may cause some contamination from higher-order nonlinear signals (Bittner et al. 1994). While clean single-exciton signals are usually desired, sometimes higher-order dynamics such as exciton-exciton annihilation can also provide insightful sample dynamics information. Recently, Malý et al. (2023) developed a method that enables to perform pump-probe measurements at higher pump intensities using the pump-intensity cycling method and arithmetically combine the datasets to extract clean single-exciton and multi-exciton signals (Malý et al. 2023). The method has the advantage of improved signal-to-noise ratio and provides a straightforward way to separate third and higher-order dynamics. We have applied this method to our room temperature data to explore how much the dynamics are contaminated by annihilation.

As such, a clean third-order non-linear transient absorption dataset can be obtained to determine decay lifetimes free of multi-exciton dynamics. Such single-exciton dynamics are related to the third-order nonlinear signal and is termed the $PP^{(3)}$ dataset. A fifth-order non-linear dynamics can also be extracted and is termed the $PP^{(5)}$ dataset, which also comprises the 3rd-order non-linear signals. The $PP^{(5)}$ signals can be analyzed to determine exciton-exciton annihilation rates. The equations used to extract the $PP^{(3)}$ and $PP^{(5)}$ signals, respectively, are:

$$PP^{(3)} = 2PP(I) - {}^{2}/_{3}\,PP(3I) + {}^{1}/_{4}\,PP(4I)$$

$$PP^{(5)} = -{}^{7}/_{6}\,PP(I) + {}^{5}/_{6}\,PP(3I) - {}^{1}/_{3}\,PP(4I).$$

We performed pump-probe measurements at three different pump intensities to obtain the $PP^{(3)}$ and $PP^{(5)}$ signals for each sample at room temperature. Fig. 7 shows the kinetic traces obtained from averaging over the Chl-*a* Q_y band (665-683 nm) for the minimum (I) and maximum ($4I$) intensities used in the intensity cycling experiment for both F680 and F730 samples. We note that for the F680 sample, the used intensity range does not induce significant change in dynamics, but we did not want to deviate significantly from the intensities used in transient absorption experiments described above. The extracted $PP^{(3)}$ and $PP^{(5)}$ signals are in Fig. 7 also shown for both samples. The kinetic trace measured at 41μJ/cm^2, the least pulse energy density used in each sample measurement, is plotted in the same graphs as a reference for effective $PP^{(3)}$ extraction. Note that while for the F680 sample the 41μJ/cm^2 kinetic corresponds to the base intensity I used in the intensity cycling experiment, for the F730 sample it is even less than the base intensity. The $PP^{(3)}$ trace should not decay faster than the traces

obtained at 41μJ/cm^2 because it is free of higher-order nonlinear dynamics. Indeed, in both samples, the PP3 signal does not decay faster than the reference, hence we are confident of effective third-order nonlinear signal extraction.

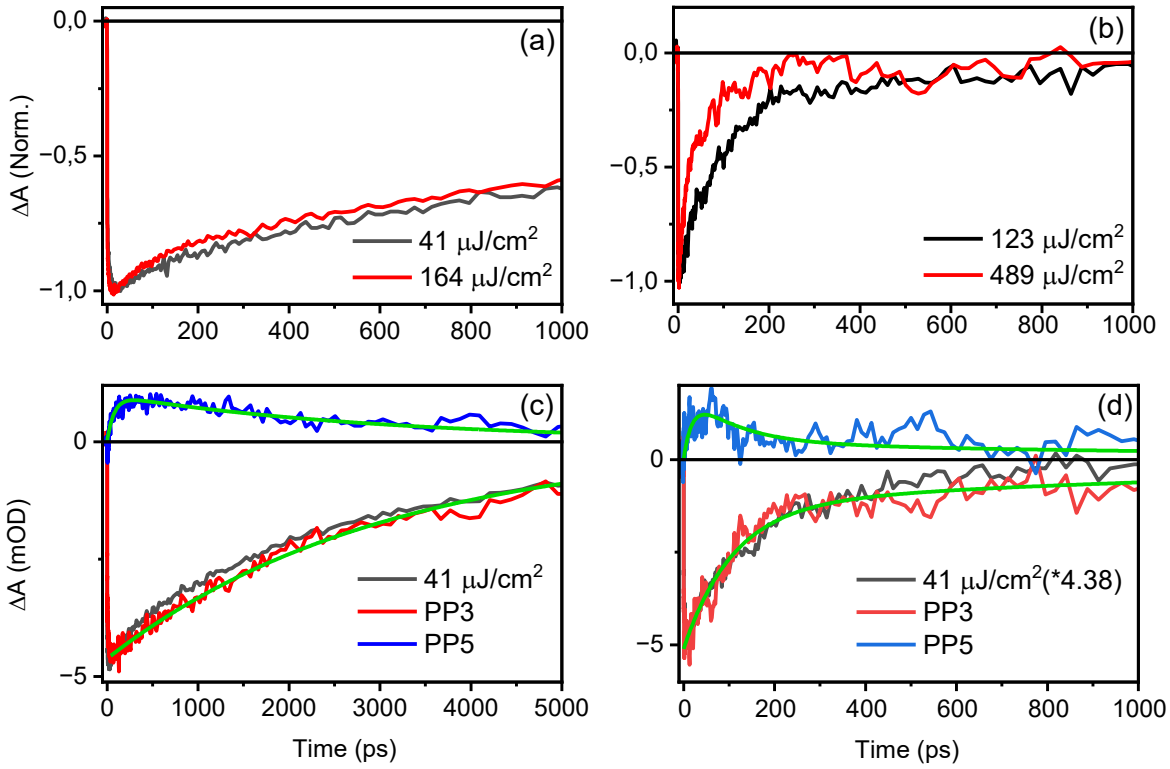

Figure 7. Normalized Chl-*a* Q_y kinetic traces measured at minimal (*I*) and maximal (4*I*) excitation intensities for F680 (a) and F730 (b) samples. The extracted PP$^{(3)}$ and PP$^{(5)}$ signals compared to the 41 μJ/cm^2 kinetic trace for F680 (c) and F730 (d) samples. The solid lines in panels (c) and (d) are fits of the PP3 and PP5 signals. All data shown in the figure were obtained by averaging the kinetics over the 665-683 nm spectral region.

The PP$^{(3)}$ and PP$^{(5)}$ signals were fitted as shown in Fig. 7 to determine the average PP$^{(3)}$ lifetime and the exciton-exciton annihilation rate constants in the

respective samples. To determine the annihilation rate, *k*, the PP$^{(5)}$ signal has been fitted with a 3D diffusion model of the form

$$PP^5 = (1 - exp^{-kt}) \times D(t)$$

The decay kernel, $D(t)$ is constructed from the fitting parameters of the PP$^{(3)}$ signal and has the form (Malý et al. 2023)

$$D(t) = a_1 exp^{-\tau_1 t} + a_2 exp^{-\tau_2 t}$$

The fitting parameters are summarized in Table 2. We obtained the average annihilation-free lifetimes of 3 ns and 436 ps for F680 and F730, while the annihilation time constants yielded to 81 and 22 ps for the F680 and F730 samples, respectively. The value of 81 ps obtained for the F680 samples is longer than that obtained for LHCII trimers by Malý et al. (2023), but it is comparable to previously reported values in literature such as 86 ps (Rutkauskas et al. 2012). The transient absorption data presented in Figs 4-6 and used for global analysis (Fig. S4) were measured with 60-70 μJ/cm^2 fluence, thus, based on data shown in Fig. 7 the TA data contain some annihilation component. However, as evidenced by the above analysis, the presence of the annihilation component affects the overall Chl-*a* decay only mildly and certainly is not the reason for the significantly shorter Chl-*a* lifetime in F730.

Table 2: F680 and F730 PP$^{(3)}$ and PP$^{(5)}$ fitting parameters. The parameters a_1, a_2, τ_1, and τ_2 are obtained from an exponential model fit of the PP$^{(3)}$ Chl-*a* Q_y at bleaching maximum, and used in constructing the decay kernel for fitting the PP$^{(5)}$ kinetic to determine the annihilation time constant, τ_{an}.

	PP3 fitting					**PP5 fitting**
Sample	a_1	τ_1	a_2	τ_2	τ_{ave}	τ_{an}
F680	--	--	-4.6 x 10^{-3}	3.0 ns	3.0 ns	81 ps
F730	-3.9 x 10^{-3}	108 ps	-1.2 x 10^{-3}	1.5 ns	433 ps	22 ps

Carotenoid spectra

In contrast to TRF, TA can provide information about spectral properties of carotenoids in F680 and F730. To obtain spectral profile of the characteristic S_1-S_n band of carotenoids, we have excited F680 and F730 at 77 K at 490 nm, where the carotenoid absorption dominates. TA spectra measured at 1 ps after excitation are shown in Fig. 8a. The carotenoid S_1-S_n band spans the 520-600 nm spectral region, and for F680, two distinct shoulders at 548 and 566 nm are visible. These shoulders merge to a single band in F730 peaking around 560 nm. The inset of Fig. 8a, which zooms in to the S_1-S_n band normalized to maximum, clearly shows that the aggregation of LHCII in F730 induces a red shift of the S_1-S_n band. The strong Chl-*a* bleaching at 1 ps after carotenoid excitation reflects efficient carotenoid-to-Chl energy transfer via the S_2 state, which is the main route in LHCII (Croce et al. 2001; Van Amerongen and Van Grondelle 2001). The appearance of Chl-*b* bleaching confirms that carotenoids in LHCII transfer energy also to Chl-*b*, though a fraction of the Chl-*b* signal could be due to direct excitation of Chl-*b*

which still has some absorption at 490 nm (Croce et al. 2001; Van Amerongen and Van Grondelle 2001).

Even though there is no presence of carotenoid triplet after excitation of Chl-*b* by 100 fs pulses, using microsecond excitation, which essentially mimics continuous excitation, can accumulate carotenoid triplet even in F730 LHCII. This is demonstrated in Fig 8b which shows normalized room temperature microsecond ^{3}Car T-S spectra for the F680 and F730 samples. In both cases, besides the typical triplet-triplet absorption peak, the spectra contain Chl-*a* bleaching signal, which is located at 678 and 684 nm for the F680 and F730 samples. This bleaching signal is the well-known 'interaction peak that originates from the interaction between carotenoid triplet and Chl-*a* (Migliore et al. 2023). The 6 nm red-shift of the interaction peak in F730

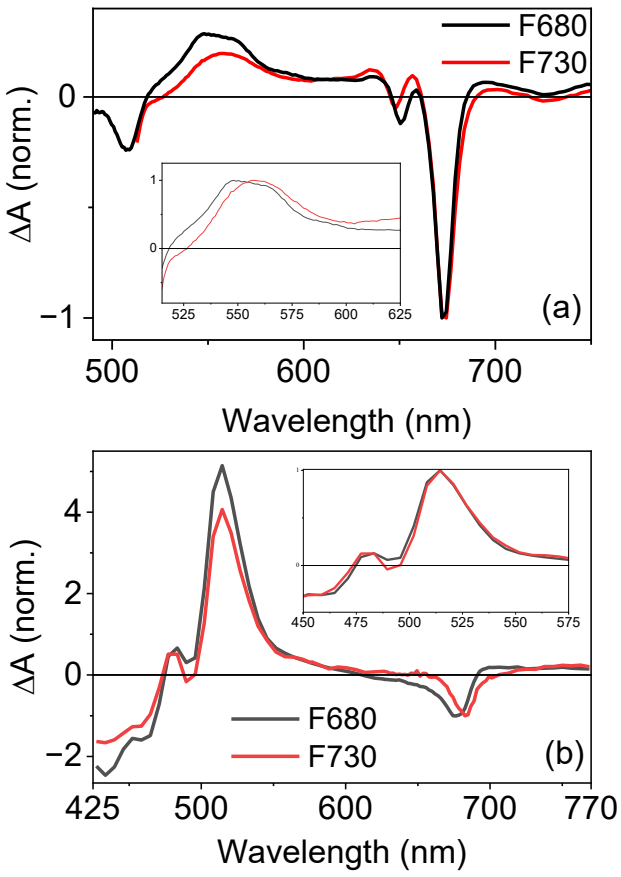

Figure 8. (a) Transient absorption spectra of F680 and F730 at 77 K at 1 ps after excitation of carotenoids at 490 nm. Spectra are normalized to Chl-*a* bleaching, inset shows magnification of the carotenoid S_1-S_n band normalized to maximum. (b) Room temperature T-S spectra of the F680 and F730 samples recorded at 4 µs after excitation by a 2 µs broadband pulse. The spectra are normalized at the Chl-*a* interaction peak maximum, while the inset compares the two spectra normalized at the maximum of the carotenoid triplet signal.

indicates that LHCII aggregation affects Chl-*a* molecules interacting with carotenoid triplets. On the other hand, the carotenoid triplet-triplet absorption peaks centered at 514 nm are identical for the two samples as shown in the inset, indicating that carotenoids involved in triplet protection are not affected by aggregation.

Discussion

The glycerol-treated LHCII complexes provide a suitable model for studying the red emitting states (RES) generated upon aggregation as the glycerol treatment significantly enhances the amplitude of the red emission at 77 K, which is even stronger than the 'standard' 680 nm emission (Fig. 1). These samples resemble the lincomycin-treated Arabidopsis plants, which lacks PSI and reaction center of PSII, and consist of thylakoid membranes packed by LHCII (Chmeliov et al. 2019). The combination of time-resolved fluorescence and ultrafast transient absorption spectroscopy used here offers further insight into possible origin of the red emission as most studies carried out so far relied solely on time-resolved fluorescence (Miloslavina et al. 2008; Chmeliov et al. 2019; Tutkus et al. 2021). To identify a possible contribution from annihilation processes, which are inevitably present in transient absorption experiments, we have applied intensity cycling method to our room temperature data to isolate the annihilation-free decays of excited Chl-*a* in transient absorption experiments.

Dynamic processes occurring in F680 and F730 at time scales <50 ps are mostly associated with Chl-*b* to Chl-*a* energy transfer (also carotenoid-Chl energy transfer in time resolved fluorescence where 480 nm was used for excitation), and equilibration processes within the Chl-*a* pool in LHCII as evidenced also by red shift of the Chl-*a* bleaching maximum shown in Fig. S2. At room temperature, the sub-10 ps lifetimes extracted from fitting the transient absorption data are associated with Chl-*b* to Chl-*a* energy transfer in both F680 and F730. Yet, the time components having 86 ps (F680) and 22 ps (F730) lifetimes obtained from global fitting of transient absorption data (Fig. S4) reasonably match the annihilation time constants of 81 and 22 ps extracted from fitting the PP5 dataset in the intensity-cycling experiment (Table 2). We thus assign these components as predominantly due to annihilation, which is also supported by significantly larger amplitude of this component in F730. For aggregated sample the contribution of annihilation is expected to be larger. On the other hand, the final EADS with lifetimes 2.4 ns (F680) and 176 ps (F730) have their counterparts in dominating time components of annihilation-free kinetics (PP3), which contain time components of 3 ns (F680)

and 108 ps (F730) as indicated in Table 2. In TR-fluorescence (Table 1), room temperature decay of F730 contains a dominant component ~120 ps, which correspond reasonably to the 108 ps component in the annihilation-free transient absorption data (Table 2). F680 exhibits a single exponential 4 ns lifetime, again reflecting the longest decay component from transient absorption. Thus, all experiments carried out at room temperature indicate that in F730 Chl-*a* is significantly quenched, yielding average lifetime of hundreds of ps and this lifetime shortening is not caused by annihilation.

At 77 K, F680 exhibits essentially the same behavior as at room temperature except slower decay (6 ns) in TR-fluorescence. This prolongation of Chl-*a* lifetime is not captured by transient absorption, most likely due to the limited time window of the experiment. The F730 LHCII however, has in TR-fluorescence complicated multi-exponential decay pattern consisting of at least four components which have significantly different spectra (Table 1 and Fig. 3). Comparison of these decay components with transient absorption (omitting the fastest components related to inter-complex energy transfer and equilibration) shows that the 170 ps component from TR-fluorescence has a counterpart in 54 ps component in TA. Both dominate in the spectral region around 680 nm, and their difference is likely caused by presence of annihilation in TA data. The next TR-fluorescence component, 600 ps, has maximal amplitude around 700 nm, and nearly identical component, 670 ps, is also extracted from TA data. In TA global fitting (Fig. S4), this component also has a red tail extending beyond 700 nm, resembling the spectral shape of the 600 ps component in TR-fluorescence.

Even though we can reasonably match the decay components obtained from TRF and TA experiments, the main motivation to do TA experiments along with TRF was to search for long-lived signals in TA that could be associated with excited states/species responsible for the red emission. Unfortunately, no such signals appear in our transient absorption data, neither do we see any signals attributable to a quencher. The absence of long-lived signals in TA data, even if they are detected in TR-fluorescence (Fig. 3), implies that the state(s) responsible for the red emission have a low transition dipole moment and/or number of the red emitting Chl-*a* in the LHCII aggregate is low. This is also obvious from DAS obtained from TRF: amplitudes of decay components associated with red emitting states are much lower than those associated with 680 nm emission (Fig. 3). In fact, in TA data we can resolve the 600 ps decay component from TRF, which has the largest amplitude from the red-shifted TRF decay components. The spectral shape of the 600 ps DAS in Fig. 3 matches well the shape of the Chl-*a* bleaching in the 672 ps EADS shown in Fig. S4d. The two nanosecond DAS, however, are not detected in

TA, most likely due to their low amplitude which prevents seeing them in TA due to limited S/N ratio of TA experiment.

The observed behavior of RES is consistent with previous assignments of these states to either Chl-Chl charge transfer states (Müller et al. 2010; Chmeliov et al. 2016; Ostroumov et al. 2020; Yao et al. 2022) or excimers (Ruban and Saccon 2022; Wilson et al. 2022, Zou et al. 2025) as precise distinction between these two excited-state species is complicated and both can actually contribute to the excited-state character (Young and Wasielewski 2020). RES in LHCII likely have low transition dipole moment for the transition from these states to the ground state as evidenced by hole-burning experiments revealing large electron-phonon coupling for the red states in LHCII aggregates (Kell et al. 2014). This large coupling leads to a large Huang-Rhys factor, which is a measure of displacement of potential minima in the ground and excited states, resulting in significant redshift of RES emission. Our data are fully consistent with this interpretation. Similar behavior related to light-harvesting complexes may be traced in intramolecular charge transfer states in keto-carotenoids, which also exhibit weak and significantly red-shifted emission (Polívka et al. 2007). Yet, in keto-carotenoids the CT states exhibit strong excited-state absorption which is not observed for Chl RES in LHCII as evidenced by absence of any long-lived ESA signals in our TA data on F730 (Fig. 5, Fig. S1).

Interestingly, we have not unambiguously detected any time component attributable to energy transfer from Chl-*a* emitting around 680 nm to RES, except possibly the 50 ps component that could be associated with a formation of the red-shifted Chl-*a* bleaching in transient absorption spectra, which, however, certainly contains also some annihilation component. Yet, it seems that equilibration within the Chl-*a* pool occurs alongside the formation of all red-shifted CT states that subsequently decay in parallel with different lifetimes. The difference in lifetime and spectra of individual CT states represented by DAS in Fig. 3 would then correspond to different aggregation forms of LHCII in F730 rather than to different RES within one LHCII aggregate. Both TRF and TA data also suggest that all RES in LHCII are populated within the first 50 ps at 77 K, which is consistent with the model proposed by Ostroumov et al. (Ostroumov et al. 2020), but it does not match the ~200 ps lifetime of the 680 nm Chl-*a*, preventing to assign the quenching of 680 nm Chl-*a* at 77 K to a simple energy transfer from the blue to red Chl-*a* states.

There is no doubt that the aggregated LHCII in F730 is quenched, thus the presence of low temperature red emission is associated with quenching. Yet, the quenching mechanism and origin of the quencher remains a matter of debate. While the first studies assigning the RES to

Chl-Chl CT states also identified these states as quenchers (Miloslavina et al. 2008; Holzwarth et al. 2009), later studies suggested that the presence of RES states is only a marker of quenching process with no direct involvement in quenching, which was assigned to energy transfer from Chl-*a* to carotenoid instead (Chmeliov et al. 2016, 2019). The strong temperature dependence of Chl-*a* red emission implies that the RES population is stable only at low temperature. With increasing temperature, back transfer to "blue" Chl-*a* emitting around 680 nm must occur and at room temperature, equilibrium between blue and red emitting chlorophylls is heavily shifted towards the blue ones, preventing observation of red emission at room temperature (Yao et al. 2022). This however contrasts to nearly temperature independent quenching of Chl-*a* in F730: the 680 nm Chl-*a* has ~200 ps lifetime at both 77 and 293 K (Table 1). Thus, even if there is essentially no RES population at room temperature (Chmeliov et al. 2016, 2019), the quenching is the same as at 77 K when the RES population is significantly larger. Thus, the quenching capacity is not correlated with RES population manifested by amplitude of the red emission, speaking rather against the hypothesis identifying CT states as the quencher in LHCII.

The other hypothesis proposes that the quencher in aggregated LHCII is the carotenoid S_1 state that accepts energy from the Q_y state of the 680 nm Chl-*a* (Chmeliov et al. 2019). This mechanism has been demonstrated to work in some specific high light induced proteins (Hlips) (Staleva et al. 2015; Skotnicová et al. 2021) and earlier, based on kinetic modelling, suggested to operate also in LHCII (Ruban et al. 2007). In LHCII, to reliably identify this mechanism is experimentally demanding because, in contrast to Hlips, the lifetime of the quencher (presumably lutein) is much shorter (~10 ps) than the quenching time (~250 ps), making the population of the quencher very low and hardly detectable (Ruban et al. 2007).

To operate efficiently, this mechanism requires the carotenoid S_1 state low enough to allow energy transfer from excited Chl-*a*, and in Hlips, in which it operates efficiently, this condition is ensured by significant red shift of carotenoid absorption spectrum compared to unquenched complexes (Skotnicová et al. 2021). Therefore, if this mechanism should work in F730, the carotenoid spectrum should be red shifted compared to F680. This is indeed observed in TAS for the S_1-S_n band (Fig. 8a) and some extra absorption at the low energy side of the carotenoid band above 500 nm is also visible in absorption spectrum, but only at 77 K (Fig. 1a). However, room temperature absorption spectrum does not show anything comparable, even though F730 is clearly quenched at room temperature. Conclusion that the aggregation-induced quenching is likely unrelated to carotenoid S_1 state is also supported by data reported on LHCII from the

green alga *Bryopsis corticulans* (Yao et al. 2022). The LHCII from Bryopsis contains carotenoids siphonein and siphonaxanthin that both have the S_1 energy significantly higher than lutein, which is the expected quencher in plant LHCII (Ruban et al. 2007), yet the Bryopsis LHCII exhibit presence of RES (though weaker than observed here) and quenching upon aggregation (Yao et al. 2022).

Alternatively, a few recent studies targeting CP29 (Mascoli et al. 2019; Accomasso et al. 2024) and LHCII (Liguori et al. 2017) suggested that the quencher is a carotenoid in a specific conformation associated with S* state. The exact origin of this state is still a matter of debate (Balevičius et al. 2016), but its spectral signature is readily identified in TAS as it exhibits an excited state absorption band blue shifted in respect to the S_1-S_n carotenoid band. Thus, the S* quenching would explain the absence of the significant red shift of the carotenoid bands in LHCII, which is typical for Hlips where the S_1 quenching operates efficiently. Yet, no hint of a carotenoid signal attributable to the quencher is detected in our TAS obtained after Chl excitation (Fig. S1, Fig. S3), thus our data provides no direct experimental evidence for the hypothesis of energy transfer quenching via the S_1 or S* state of carotenoid in aggregated LHCII.

Although we cannot provide evidence for either quenching mechanism or we cannot identify the quencher, TA spectra shown in Fig. 8 demonstrate that there must be some local conformational changes upon aggregation. Besides the additional red-shifted bleaching signal in F730 shown in Fig. 5, the carotenoid transient absorption spectra in Fig. 8 provide the only reliable difference between F680 and F730 samples, indicating that the carotenoid-protein and carotenoid-Chl interaction are affected upon aggregation. The shape of the Chl interaction peak in T-S spectra (Fig. 8b) is very sensitive to mutual configuration of lutein in L1 site and three closely positioned Chls 610/611/612 as well as the local environment of this pigment cluster (Migliore et al. 2023). The clear change in shape and position of the interaction peak thus points to this cluster as a site that could be responsible for quenching. This agrees with earlier assignment (Ostroumov et al. 2020), yet the precise mechanism as well as the quencher remain hidden, because neither the hypothesis of CT state as the quencher nor the energy transfer quenching via the carotenoid S_1 state are fully consistent with data.

The final resolution of this problem is thus left for further studies. To successfully and reliably find the answer to the question of how the aggregation-induced low temperature emission in LHCII is related to quenching, the key step forward seems to be better characterization of the aggregated LHCII samples. Various LHCII preparations with 77 K red

emission have been reported, including the glycerol-treated samples reported here or in (Wilson et al. 2022), lincomycin-treated chloroplasts (Chmeliov et al. 2019), LHCII in proteoliposomes (Wilson et al. 2022) or just by removing detergent without further treatment to induce aggregation (Ostroumov et al. 2020). It is important to note that even though all the reported preparations exhibit clear red emission at 77 K, spectral properties (maxima, bandwidths) as well as amplitudes relative to the 680 nm emission vary significantly among various preparations. This suggests that the size and/or internal organization of LHCII aggregates strongly depends on preparation method and at least some preparations may be largely heterogeneous in terms of aggregate size, making modelling the quenching pathways and mechanisms very complicated. Thus, better control over the LHCII aggregate formation is clearly needed and for example single molecule spectroscopy holds promise to fulfill this task.

Statements and Declaration

Competing Interests. The authors declare no competing interests.

Funding. The authors from University of South Bohemia thank the Czech Science foundation grant 24-11344S and OP JAK project Photomachines reg. no. CZ.02.01.01/00/22_008/0004624.

Data Availability Statement. All key data are presented in the manuscript or Supporting Information. Raw spectroscopic data are available from authors upon request.

Author Contribution Statement. A.R. and T.P. designed the study; V.S., V.K. and A.P. performed ultrafast transient absorption experiments; V.S. analyzed all ultrafast transient absorption data; A.P. performed and analyzed the intensity cycling experiment; D-H.L. and D.B. prepared the samples; D.B. performed and analyzed time-resolved fluorescence experiments; V.S, T.P., A.R.,A.P. and DB wrote the manuscript draft, all authors contributed to the finalization of the manuscript.

References

Accomasso D, Londi G, Cupellini L, Mennucci B (2024) The nature of carotenoid S* state and its role in the nonphotochemical quenching of plants. Nat Commun 15:847. https://doi.org/10.1038/s41467-024-45090-9

Alster J, Bína D, Charvátová K, Lokstein H, Pšenčík J (2024) Direct observation of triplet energy transfer between chlorophylls and carotenoids in the core antenna of photosystem I from *Thermosynechococcus elongatus*. Biochimica et Biophysica Acta (BBA) – Bioenergetics 1865: 149016. https://doi.org/10.1016/j.bbabio.2023.149016.

Balevičius V, Abramavicius D, Polívka T, et al (2016) A unified picture of S∗ in carotenoids. Journal of Physical Chemistry Letters 7:3347–3352. https://doi.org/10.1021/acs.jpclett.6b01455

Barzda V, Gulbinas V, Kananavicius R, et al (2001) Singlet-singlet annihilation kinetics in aggregates and trimers of LHCII. Biophys J 80:2409–2421. https://doi.org/10.1016/S0006-3495(01)76210-8

Belgio E, Johnson MP, Jurić S, Ruban A V. (2012) Higher plant photosystem II light-harvesting antenna, not the reaction center, determines the excited-state lifetime - Both the maximum and the nonphotochemically quenched. Biophys J 102:2761–2771. https://doi.org/10.1016/j.bpj.2012.05.004

Bína D, Litvín R, Vácha F, Šiffel P (2006) New multichannel kinetic spectrophotometer-fluorimeter with pulsed measuring beam for photosynthesis research. Photosynth Res 88:351–356. https://doi.org/10.1007/s11120-006-9071-y

Bittner T, Irrgang K-D, Renger G, Wasielewski MR (1994) Ultrafast excitation energy transfer and exciton-exciton annihilation processes in isolated light harvesting complexes of photosystem II (LHC II) from spinach. J Phys Chem 98:11821–11826. https://doi.org/10.1021/j100097a004

Bode S, Quentmeier CC, Liao PN, et al (2009) On the regulation of photosynthesis by excitonic interactions between carotenoids and chlorophylls. Proc Natl Acad Sci U S A 106:12311–12316. https://doi.org/10.1073/pnas.0903536106

Chmeliov J, Gelzinis A, Franckevičius M, et al (2019) Aggregation-related nonphotochemical quenching in the photosynthetic membrane. Journal of Physical Chemistry Letters 10:7340–7346. https://doi.org/10.1021/acs.jpclett.9b03100

Chmeliov J, Gelzinis A, Songaila E, et al (2016) The nature of self-regulation in photosynthetic light-harvesting antenna. Nat Plants 2:16045. https://doi.org/10.1038/nplants.2016.45

Croce R, Müller MG, Bassi R, Holzwarth AR (2001) Carotenoid-to-chlorophyll energy transfer in recombinant major light-harvesting complex (LHCII) of higher plants. I. Femtosecond transient absorption measurements. Biophys J 80:901–915. https://doi.org/10.1016/S0006-3495(01)76069-9

Croce R, Van Amerongen H (2014) Natural strategies for photosynthetic light harvesting. Nat Chem Biol 10:492–501. https://doi.org/10.1038/nchembio.1555

Demmig-Adams B (1990) Carotenoids and photoprotection in plants: A role for the xanthophyll zeaxanthin. Biochimica et Biophysica Acta (BBA) - Bioenergetics 1020:1–24. https://doi.org/10.1016/0005-2728(90)90088-L

Frank HA, Cua A, Chynwat V, et al (1994) Photophysics of the carotenoids associated with the xanthophyll cycle in photosynthesis. Photosynth Res 41:389–395. https://doi.org/10.1007/BF02183041

Holt NE, Zigmantas D, Valkunas L, et al (2005) Carotenoid cation formation and the regulation of photosynthetic light harvesting. Science (1979) 307:433–436. https://doi.org/10.1126/science.1105833

Holzwarth AR, Miloslavina Y, Nilkens M, Jahns P (2009) Identification of two quenching sites active in the regulation of photosynthetic light-harvesting studied by time-resolved fluorescence. Chem Phys Lett 483:262–267. https://doi.org/10.1016/j.cplett.2009.10.085

Kell A, Feng X, Lin C, et al (2014) Charge-transfer character of the low-energy Chl a Qy absorption band in aggregated light harvesting complexes II. Journal of Physical Chemistry B 118:6086–6091. https://doi.org/10.1021/jp501735p

Kirchhoff H, Hinz HJ, Rösgen J (2003) Aggregation and fluorescence quenching of chlorophyll a of the light-harvesting complex II from spinach in vitro. Biochim Biophys Acta Bioenerg 1606:105–116. https://doi.org/10.1016/S0005-2728(03)00105-1

Krüger TPJ, Novoderezhkin VI, Ilioaia C, Van Grondelle R (2010) Fluorescence spectral dynamics of single LHCII trimers. Biophys J 98:3093–3101. https://doi.org/10.1016/j.bpj.2010.03.028

Lee T-Y, Lam L, Patel-Tupper D, et al (2024) Chlorophyll to zeaxanthin energy transfer in nonphotochemical quenching: An exciton annihilation-free transient absorption study.

Proceedings of the National Academy of Sciences 121:. https://doi.org/10.1073/pnas.2411620121

Liguori N, Xu P, Van Stokkum IHM, et al (2017) Different carotenoid conformations have distinct functions in light-harvesting regulation in plants. Nat Commun 8:. https://doi.org/10.1038/s41467-017-02239-z

Liu Z, Yan H, Wang K, et al (2004) Crystal structure of spinach major light-harvesting complex at 2.72 Å resolution. Nature 428:287–292. https://doi.org/10.1038/nature02373

Malý P, Lüttig J, Rose PA, et al (2023) Separating single- from multi-particle dynamics in nonlinear spectroscopy. Nature 616:280–287. https://doi.org/10.1038/s41586-023-05846-7

Mascoli V, Gelzinis A, Chmeliov J, et al (2020) Light-harvesting complexes access analogue emissive states in different environments. Chem Sci 11:5697–5709. https://doi.org/10.1039/d0sc00781a

Mascoli V, Liguori N, Xu P, et al (2019) Capturing the quenching mechanism of light-harvesting complexes of plants by zooming in on the ensemble. Chem 5:2900–2912. https://doi.org/10.1016/j.chempr.2019.08.002

Migliore A, Corni S, Agostini A, Carbonera D (2023) Unraveling the electronic origin of a special feature in the triplet-minus-singlet spectra of carotenoids in natural photosystems. Physical Chemistry Chemical Physics 25:28998–29016. https://doi.org/10.1039/d3cp03836j

Miloslavina Y, Wehner A, Lambrev PH, et al (2008) Far-red fluorescence: A direct spectroscopic marker for LHCII oligomer formation in non-photochemical quenching. FEBS Lett 582:3625–3631. https://doi.org/10.1016/j.febslet.2008.09.044

Mirkovic T, Ostroumov EE, Anna JM, et al (2017) Light absorption and energy transfer in the antenna complexes of photosynthetic organisms. Chem Rev 117:249–293

Müller MG, Lambrev P, Reus M, et al (2010) Singlet energy dissipation in the photosystem II light-harvesting complex does not involve energy transfer to carotenoids. ChemPhysChem 11:1289–1296. https://doi.org/10.1002/cphc.200900852

Mullineaux CW, Pascal AA, Horton P, Holzwarth AR (1993) Excitation-energy quenching in aggregates of the LHC II chlorophyll-protein complex: a time-resolved fluorescence

study. Biochimica et Biophysica Acta (BBA) - Bioenergetics 1141:23–28. https://doi.org/10.1016/0005-2728(93)90184-H

Natali A, Gruber JM, Dietzel L, et al (2016) Light-harvesting Complexes (LHCs) cluster spontaneously in membrane environment leading to shortening of their excited state lifetimes. Journal of Biological Chemistry 291:16730–16739. https://doi.org/10.1074/jbc.M116.730101

Ostroumov EE, Götze JP, Reus M, et al (2020) Characterization of fluorescent chlorophyll charge-transfer states as intermediates in the excited state quenching of light-harvesting complex II. Photosynth Res 144:171–193. https://doi.org/10.1007/s11120-020-00745-8

Pascal AA, Liu Z, Broess K, et al (2005) Molecular basis of photoprotection and control of photosynthetic light-harvesting. Nature 436:134–137. https://doi.org/10.1038/nature03795

Peterman EJG, Gradinaru CC, Calkoen F, et al (1997) Xanthophylls in light-harvesting complex II of higher plants: Light harvesting and triplet quenching. Biochemistry 36:12208–12215. https://doi.org/10.1021/bi9711689

Polívka T, Hiller RG, Frank HA (2007) Spectroscopy of the peridinin-chlorophyll-a protein: Insight into light-harvesting strategy of marine algae. Arch Biochem Biophys 458:111–120. https://doi.org/10.1016/j.abb.2006.10.006

Polívka T, Zigmantas D, Sundström V, et al (2002) Carotenoid S1 state in a recombinant light-harvesting complex of photosystem II. Biochemistry 41:439–450. https://doi.org/10.1021/bi011589x

Ruan M, Li H, Zhang Y, et al (2023) Cryo-EM structures of LHCII in photo-active and photo-protecting states reveal allosteric regulation of light harvesting and excess energy dissipation. Nat Plants 9:1547–1557. https://doi.org/10.1038/s41477-023-01500-2

Ruban AV, Rees D, Noctor GD, et al (1991) Long-wavelength chlorophyll species are associated with amplification of high-energy-state excitation quenching in higher plants. Biochimica et Biophysica Acta (BBA) - Bioenergetics 1059:355–360. https://doi.org/10.1016/S0005-2728(05)80221-X

Ruban A V. (2016) Nonphotochemical chlorophyll fluorescence quenching: Mechanism and effectiveness in protecting plants from photodamage. Plant Physiol 170:1903–1916. https://doi.org/10.1104/pp.15.01935

Ruban A V. (2024) Unveiling the atomic-scale transition between light harvesting and photoprotective states in plant photosynthesis. Sci China Chem 67:1375–1377. https://doi.org/10.1007/s11426-023-1806-6

Ruban A V., Berera R, Ilioaia C, et al (2007) Identification of a mechanism of photoprotective energy dissipation in higher plants. Nature 450:575–578. https://doi.org/10.1038/nature06262

Ruban A V., Saccon F (2022) Chlorophyll a de-excitation pathways in the LHCII antenna. Journal of Chemical Physics 156:070902. https://doi.org/10.1063/5.0073825

Ruban A V., Young AJ, Pascal AA, Horton P (1994) The effects of illumination on the xanthophyll composition of the photosystem II light-harvesting complexes of spinach thylakoid membranes. Plant Physiol 104:227–234. https://doi.org/10.1104/pp.104.1.227

Rutkauskas D, Chmeliov J, Johnson M, Ruban A, and Valkunas L (2012), Exciton annihilation as a probe of the light-harvesting antenna transition into the photoprotective mode. Chem Phys 404: 123–128. https://doi.org/10.1016/j.chemphys.2012.05.002

Saccon F, Durchan M, Bína D, et al (2020) A protein environment-modulated energy dissipation channel in LHCII antenna complex. iScience 23:101430. https://doi.org/10.1016/j.isci.2020.101430

Schlau-Cohen GS, Yang H-Y, Krüger TPJ, et al (2015) Single-molecule identification of quenched and unquenched states of LHCII. J Phys Chem Lett 6:860–867. https://doi.org/10.1021/acs.jpclett.5b00034

Shukla MK, Watanabe A, Wilson S, et al (2020) A novel method produces native light-harvesting complex II aggregates from the photosynthetic membrane revealing their role in nonphotochemical quenching. Journal of Biological Chemistry 295:17816–17826. https://doi.org/10.1074/jbc.RA120.016181

Skotnicová P, Staleva-Musto H, Kuznetsova V, et al (2021) Plant LHC-like proteins show robust folding and static non-photochemical quenching. Nat Commun 12:6890. https://doi.org/10.1038/s41467-021-27155-1

Staleva H, Komenda J, Shukla MK, et al (2015) Mechanism of photoprotection in the cyanobacterial ancestor of plant antenna proteins. Nat Chem Biol 11:287–291. https://doi.org/10.1038/nchembio.1755

Tutkus M, Chmeliov J, Trinkunas G, et al (2021) Aggregation-related quenching of LHCII fluorescence in liposomes revealed by single-molecule spectroscopy. J Photochem Photobiol B 218:112174. https://doi.org/10.1016/j.jphotobiol.2021.112174

Van Amerongen H, Van Grondelle R (2001) Understanding the energy transfer function of LHCII, the major light-harvesting complex of green plants. Journal of Physical Chemistry B 105:604–617. https://doi.org/10.1021/jp0028406

Van Oort B, Roy LM, Xu P, et al (2018) Revisiting the role of xanthophylls in nonphotochemical quenching. Journal of Physical Chemistry Letters 9:346–352. https://doi.org/10.1021/acs.jpclett.7b03049

Van Stokkum IHM, Larsen DS, Van Grondelle R (2004) Global and target analysis of time-resolved spectra. Biochim Biophys Acta Bioenerg 1657:82–104. https://doi.org/10.1016/j.bbabio.2004.04.011

Wahadoszamen M, Berera R, Ara AM, et al (2012) Identification of two emitting sites in the dissipative state of the major light harvesting antenna. Physical Chemistry Chemical Physics 14:759–766. https://doi.org/10.1039/c1cp23059j

Wilson S, Li DH, Ruban AV (2022) The structural and spectral features of light-harvesting complex II proteoliposomes mimic those of native thylakoid membranes. Journal of Physical Chemistry Letters 13:5683–5691. https://doi.org/10.1021/acs.jpclett.2c01019

Yao HD, Li DH, Gao RY, et al (2022) A possible mechanism for aggregation-induced chlorophyll fluorescence quenching in light-harvesting complex II from the marine green alga Bryopsis corticulans. Journal of Physical Chemistry B 126:9580–9590. https://doi.org/10.1021/acs.jpcb.2c05823

Young RM, Wasielewski MR (2020) Mixed electronic states in molecular dimers: Connecting singlet fission, excimer formation, and symmetry-breaking charge transfer. Acc Chem Res 53:1957–1968. https://doi.org/10.1021/acs.accounts.0c00397

Zou JW, Li DH, Gao RY, Li YQ, Yu QR, Yu ZH, Ruban AV, Zhang JP, Zheng J (2025) Excimer and non-photochemical quenching in LHCII. J Chem Phys 163: 195104. https://doi.org/10.1063/5.0271063